NASA/TM—2015-218413

Crystallization Kinetics of Calcium-Magnesium Aluminosilicate (CMAS) Glass

Valerie L. Wiesner and Narottam P. Bansal
Glenn Research Center, Cleveland, Ohio

February 2015

NASA STI Program . . . in Profile

Since its founding, NASA has been dedicated to the advancement of aeronautics and space science. The NASA Scientific and Technical Information (STI) Program plays a key part in helping NASA maintain this important role.

The NASA STI Program operates under the auspices of the Agency Chief Information Officer. It collects, organizes, provides for archiving, and disseminates NASA's STI. The NASA STI Program provides access to the NASA Technical Report Server—Registered (NTRS Reg) and NASA Technical Report Server—Public (NTRS) thus providing one of the largest collections of aeronautical and space science STI in the world. Results are published in both non-NASA channels and by NASA in the NASA STI Report Series, which includes the following report types:

- TECHNICAL PUBLICATION. Reports of completed research or a major significant phase of research that present the results of NASA programs and include extensive data or theoretical analysis. Includes compilations of significant scientific and technical data and information deemed to be of continuing reference value. NASA counter-part of peer-reviewed formal professional papers, but has less stringent limitations on manuscript length and extent of graphic presentations.

- TECHNICAL MEMORANDUM. Scientific and technical findings that are preliminary or of specialized interest, e.g., "quick-release" reports, working papers, and bibliographies that contain minimal annotation. Does not contain extensive analysis.

- CONTRACTOR REPORT. Scientific and technical findings by NASA-sponsored contractors and grantees.

- CONFERENCE PUBLICATION. Collected papers from scientific and technical conferences, symposia, seminars, or other meetings sponsored or co-sponsored by NASA.

- SPECIAL PUBLICATION. Scientific, technical, or historical information from NASA programs, projects, and missions, often concerned with subjects having substantial public interest.

- TECHNICAL TRANSLATION. English-language translations of foreign scientific and technical material pertinent to NASA's mission.

For more information about the NASA STI program, see the following:

- Access the NASA STI program home page at http://www.sti.nasa.gov

- E-mail your question to help@sti.nasa.gov

- Fax your question to the NASA STI Information Desk at 757-864-6500

- Telephone the NASA STI Information Desk at 757-864-9658

- Write to:
  NASA STI Program
  Mail Stop 148
  NASA Langley Research Center
  Hampton, VA 23681-2199

NASA/TM—2015-218413

Crystallization Kinetics of Calcium-Magnesium Aluminosilicate (CMAS) Glass

Valerie L. Wiesner and Narottam P. Bansal
Glenn Research Center, Cleveland, Ohio

National Aeronautics and
Space Administration

Glenn Research Center
Cleveland, Ohio 44135

February 2015

Acknowledgments

The authors thank Dr. Bryan Harder and Dr. Dongming Zhu for helpful discussions, Dr. Richard Rogers for XRD assistance, Mr. Dereck Johnson for DTA, Dr. Paul Angel for melting the synthetic sand into glass, Mr. Ray Babuder for assistance with grinding of the bulk glass and Ms. Joy Buehler for glass specimen preparation. A portion of this work was supported by the Pathways Program at NASA Glenn Research Center.

Level of Review: This material has been technically reviewed by technical management.

Available from

NASA STI Program
Mail Stop 148
NASA Langley Research Center
Hampton, VA 23681-2199

National Technical Information Service
5285 Port Royal Road
Springfield, VA 22161
703-605-6000

This report is available in electronic form at http://www.sti.nasa.gov/ and http://ntrs.nasa.gov/

Crystallization Kinetics of Calcium-Magnesium Aluminosilicate (CMAS) Glass

Valerie L. Wiesner and Narottam P. Bansal
National Aeronautics and Space Administration
Glenn Research Center
Cleveland, Ohio 44135

Abstract

The crystallization kinetics of a calcium-magnesium aluminosilicate (CMAS) glass with composition relevant for aerospace applications, like air-breathing engines, were evaluated using differential thermal analysis (DTA) in powder and bulk forms. Activation energy and frequency factor values for crystallization of the glass were evaluated. X-ray diffraction (XRD) was used to investigate the onset of crystallization and the phases that developed after heat treating bulk glass at temperatures ranging from 690 to 960 °C for various times. Samples annealed at temperatures below 900 °C remained amorphous, while specimens heat treated at and above 900 °C exhibited crystallinity originating at the surface. The crystalline phases were identified as wollastonite ($CaSiO_3$) and aluminum diopside ($Ca(Mg,Al)(Si,Al)_2O_6$). Scanning electron microscopy (SEM) and energy dispersive spectroscopy (EDS) were employed to examine the microstructure and chemical compositions of crystalline phases formed after heat treatment.

1.0 Introduction

Particulates, such as sand and volcanic ash, pose a significant threat to the development of next-generation, high-efficiency aircraft engines that operate at elevated temperatures (>1200 °C). When an engine ingests sand or similar small siliceous debris at temperatures above 1200 °C, the particulates transform into molten deposits of calcium-magnesium aluminosilicate (CMAS) (Refs. 1 to 3). Molten CMAS infiltrates into the porous thermal and environmental barrier coatings (TBCs, EBCs) that are used to protect silicon-based ceramic matrix composite (CMC) turbine engine components from the extreme thermal and corrosive environment encountered in flight (Refs. 4 to 6). The penetration of CMAS into the coating changes the mechanical properties of the coating, which can result in undesired stresses and can prevent the coating from surviving the severe heating and cooling cycles encountered during engine operation (Refs. 7 to 11).

Inducing CMAS crystallization has been shown to be a viable approach to mitigate the deleterious effects of CMAS attack on T/EBCs at high temperatures by limiting the depth to which CMAS may infiltrate the coating (Ref. 8). Previous T/EBC studies have developed coating materials that promote crystallization of CMAS, and these investigations have focused on evaluating the resulting phases that develop during CMAS/coating interactions (Refs. 12 to 14). Concurrently, the crystallization behavior of CMAS alone has been previously investigated for applications ranging from ceramic glazes (Ref. 15) to solid oxide fuel cell sealants (Ref. 16); however, these previous compositions are markedly different from those studied in aerospace coatings literature. Because additional compositional constituents, like potassium or sodium oxides, have a pronounced effect on CMAS crystallization (Refs. 17 and 18), understanding the crystallization behavior of CMAS compositions relevant to aerospace applications is vital to develop novel coating material systems that are resistant to CMAS interactions.

The objective of the current study was to evaluate the crystallization kinetics of a CMAS glass that was prepared by melting a synthetic sand composition by differential thermal analysis (DTA) in powder and bulk forms. Complementary heat treatments of the bulk glass were performed at various temperatures and times. X-ray diffraction was utilized to identify the resulting crystalline phases that developed within the glass. Microstructures of the heat treated CMAS specimens and compositions of the crystalline phases were analyzed using scanning electron microscopy (SEM) and energy dispersive spectroscopy (EDS).

2.0 Materials and Methods

CMAS glass was prepared by melting synthetic sand having a composition of 34 wt% quartz (SiO_2), 30 wt% gypsum ($CaSO_4 \cdot 2H_2O$), 17 wt% aplite (SiO_2+$KAlSi_3O_8$), 14 wt% dolomite ($CaMg(CO_3)_2$) and 5 wt% salt (NaCl). The synthetic sand was heated to 1550 °C with 30-min isothermal holds at 150, 790, and 1275 °C at a rate of 10 °C/min in a platinum crucible in a box furnace. After 1 h isothermal hold at 1550 °C, the melt was quenched in water. The resulting glass frit was ground to powder using a Fritsch Planetary Mono Mill Pulverisette 6 (Idar-Oberstein, Germany) with zirconia milling media in a zirconia container. The glass powder was passed through a sieve (≤297 μm mesh) to separate the fine from coarse and bulk particles. The composition of the glass powder was analyzed by a Varian Vista Pro Inductively Coupled Plasma Atomic Emission Spectrometer (ICP-AES).

Differential thermal analysis (DTA) was carried out using a Netzsch STA 409 (Burlington, MA) to evaluate the crystallization kinetics of the fine CMAS glass powder (particle size ≤297 μm) and bulk samples having a mass of approximately 100 mg. DTA scans were performed in air from room temperature to 1250 °C or 1500 °C at heating rates ranging from 2 to 50 °C/min. Alumina pans were used to contain the CMAS glass during testing. The glass transition temperatures (T_g) and crystallization peak temperatures (T_P) were determined from each DTA scan.

Bulk CMAS glass specimens weighing ~100 mg were isothermally heat treated on a platinum surface in a box furnace in air. Duplicate samples were heated at a ramp rate of 10 °C/min to a temperature ranging from 690 to 960 °C for 10 min, 1, 5 or 10 h and then cooled at 10 °C/min to room temperature. After heat treatment, one of the two glass specimens was ground using an alumina mortar and pestle. Powder X-ray diffraction (XRD) analysis (0.02°/2θ step, 2.5 s/step) was performed using a Bruker D8 Advance diffractometer with Cu Kα radiation to evaluate the development of crystalline phases in heat treated glass specimens. The second heat treated glass specimen was mounted in epoxy and polished to yield a cross-section for microstructural and compositional analysis using scanning electron microscopy (SEM) and energy dispersive spectroscopy (EDS). The polished specimen cross-sections were coated with a thin layer of carbon for electrical conductivity. A Hitachi 4700II Cold Field Emission Gun SEM (Hitachi High Technologies America, Inc., Pleasanton, CA) with EDS analyzer in secondary (SE) and back-scattered electron (BSE) imaging modes was used. The average depth of crystalline layers observed in heat treated specimens was determined by evaluating five different regions in SEM micrographs of a particular specimen and measuring the surface-initiated crystallization depth along 50 lines using ImageJ image processing and analysis software. The resulting 250 length measurements were averaged to obtain a mean crystal layer thickness for specimen at a particular heat treatment time and temperature.

3.0 Results and Discussion

3.1 Composition of Synthetic Sand and CMAS Glass

XRD spectra of the synthetic sand and CMAS glass powder are presented in Figure 1(a) and (b), respectively. XRD results confirmed the presence of quartz (SiO_2), gypsum ($CaSO_4 \cdot 2H_2O$), $KAlSi_3O_8$, dolomite ($CaMg(CO_3)_2$) and salt (NaCl) in the synthetic sand. The CMAS glass powder was amorphous as expected. The composition of the CMAS glass as analyzed by ICP-AES method was 23.3CaO-6.4MgO-3.1Al_2O_3-62.5SiO_2-4.1Na_2O-0.5K_2O (mol%) and 21.9CaO-4.3MgO-5.4Al_2O_3-63SiO_2-4.3Na_2O-0.8K_2O (wt%).

3.2 Evaluation of Crystallization Kinetics by DTA

DTA thermograms of CMAS glass powder and bulk specimens were obtained at various scan rates ranging from 5 to 50 °C/min. Representative DTA scans obtained at heating rates of 5 and 50 °C/min are shown in Figure 2(a) and (b), respectively. The endothermic peak, which was observed for both powder and bulk specimens in DTA thermograms obtained at a scan rate of 10 °C/min, at 704 °C was associated

with the glass transition (T_g). The two subsequent exothermic peaks (T_{P1} and T_{P2}, respectively) seen in DTA thermograms of glass powder corresponded to crystallization. Exothermic peak maximum temperature values for powder and bulk glass are given in Table 1. The presence of two exothermic peaks suggested the crystallization of at least two distinct phases within the glass at different temperatures (Ref. 19). The temperature range in which the first exothermic peak was observed in CMAS glass powder thermograms was ~842 to 930 °C, and the second peak was around 930 to 1024 °C. A distinct exothermic peak corresponding to T_{P1} could not be identified in DTA thermograms for bulk CMAS glass, but an exothermic peak (T_{B2}) likely corresponding to T_{P2} was apparent in all DTA scans.

The substantial shift of the second exothermic peak from lower temperatures for the glass powder to higher temperatures for the bulk glass suggested that this peak was likely associated with a crystalline phase that developed by a surface-nucleated mechanism (Ref. 19). However, further analysis is required to fully ascertain the crystallization mechanism(s) at play in the CMAS glass. When a CMAS glass of this composition would come into contact with T/EBCs at elevated temperatures, the coating might act as a nucleation site, inducing crystallization of CMAS originating at the melt/coating interface. Crystallization of CMAS glass could be promoted by introducing dopants into the coating that could initiate crystallization by a surface-nucleated mechanism. The endothermic peaks at ~1228 to 1252 °C and ~1425 to 1470 °C likely involved the melting of the crystalline phases and/or of the residual glass.

Crystallization kinetics of the CMAS glass powder were evaluated from experimental values of peak maximum temperatures (T_{P1}, T_{P2}, and T_{B2}) obtained from DTA scans at various heating rates (refer to Table 1) using an approach previously utilized by Bansal et al. (Refs. 20 to 22) The isothermal crystallization of a glass can be given by the Johnson-Mehl-Avrami (JMA) equation: (Refs. 23 to 26)

$$-\ln(1-x) = (k\,t)^n \tag{1}$$

where x represents the volume fraction of glass crystallized after time t, k is the reaction-rate constant and n is the Avrami exponent, which is a dimensionless quantity that is associated with the morphology of crystal growth. The Arrhenius equation can be used to express the temperature dependence of k within narrow temperature ranges and can be written as

$$k = \nu\, \exp(-E/RT) \tag{2}$$

where ν is an effective frequency factor, E is the activation energy of the transformation, R represents the gas constant and T is the absolute temperature at which the transformation occurs.

During DTA scans, the temperature of the sample varies at a constant rate, θ , which can be defined as the change in temperature with respect to time ($\theta = dT/dt$), such that θ can be related to the temperature, T, after a certain time, t, and the initial temperature, T_i, by the following expression:

$$T = T_i + \theta t \tag{3}$$

Consequently, the reaction rate constant, k, as given in Equation (2), can now be expressed as a time-dependent variable for the non-isothermal case using Equation (3):

$$k(t) = \upsilon\, \exp\left(-\frac{E}{R(T_i + \theta t)}\right) \tag{4}$$

The JMA equation can thus be written in integral form as

$$-\ln(1-x) = \left(\int_0^t k(t)\right)^n \tag{5}$$

By applying the Borchardt assumption (Ref. 27), which implies that the instantaneous reaction rate is proportional to the displacement of the DTA trace from its baseline, the maximum rate of transformation occurs at the exothermic crystallization peak. Bansal et al. (Refs. 20 to 22) have shown that the temperature, T_P, of the crystallization peak varies with respect to the heating rate, θ, by

$$\ln\left(\frac{T_P^2}{\theta}\right) = \ln\left(\frac{E}{R\nu}\right) + \frac{E}{RT_P} \tag{6}$$

As a result, a plot of $\ln(T_P^2/\theta)$ versus $1 / T_P$ will be linear with slope of E/R and an intercept of $(\ln(E/R) - \ln \nu)$.

Plots of $\ln(T_P^2/\theta)$ versus $1 / T_P$ for each exothermic peak were linear as shown in Figure 3(a) and (b). A linear least squares fitting was applied to the experimental data to obtain values for the activation energy and frequency factor for both exothermic peaks. The correlation coefficient, R^2, was greater than 0.99 for both plots shown in Figure 3(a) and (b). Table 2 shows the activation energy and frequency factor parameters calculated for CMAS glass in powder and bulk forms. The activation energies for the first and second exothermic peaks were 263 and 294 kJ/mol, respectively, for the glass powder. The activation energy for the exothermic peak (T_{B2}) for the bulk glass was found to be 286 kJ/mol. This value was slightly lower than that for the glass powder, which was expected, because the powder had a higher surface area due to the smaller particle size, and the bulk specimens required fewer nucleation sites to initiate crystallization. Although not directly comparable due to compositional variance, previous studies have reported similar activation energy values for other CMAS glass compositions (Refs. 15, 28, and 29). Because asymmetric exothermic peaks were observed in DTA thermograms at varying scan rates, as highlighted in Figure 2(a) and (b), *n* could not be calculated by the Piloyan approach (Ref. 30).

3.3 Development of Crystalline Phases by X-ray Diffraction

Figure 4 shows XRD spectra for glass specimens heat treated at various times and temperatures of 825 to 925 °C. XRD of specimens after heat treatments at 960 °C for various times are presented in Figure 5. Although no crystalline phases were detected in glass specimens heat treated at or below 825 °C, wollastonite ($CaSiO_3$) (PDF 04-010-0710) was detected as the major phase after annealing at and above 900 °C. Aluminum diopside ($Ca(Mg,Al)(Si,Al)_2O_6$) (PDF 01-076-2502) was determined to be the minor phase in specimens heat treated at 925 °C and above. It is unclear if the two phases correspond to a particular crystallization peak observed in DTA. The development of crystalline phases in CMAS bulk glass heat treated at temperatures ranging from 690 to 960 °C for various times is shown in Table 3. The presence of trace amounts of aluminum diopside cannot be ruled out in specimens heat treated at 900 °C for 10 h. It was difficult to confirm its presence from XRD data because of the overlap of the primary peaks of wollastonite and aluminum diopside phases and also because the crystallinity in the specimen was too small when compared with amorphous content. However, the XRD pattern for aluminum diopside provided the best fit for the minority phase in spectra of glass specimens heat treated at or above 925 °C.

At temperatures relevant to aircraft engines (>1200 °C), the viscosity of the CMAS glass will be low, causing the CMAS melt to infiltrate into open pores of T/EBC coatings. The rate at which molten CMAS infiltrates into the pores of a coating is dependent on its viscosity. Consequently, viscosity values of CMAS glass are needed at various temperatures to determine the timescale required for CMAS to penetrate a coating. However, as XRD results suggested, crystallization of bulk glass specimens could be initiated at temperatures as low as 900 °C when held for 10 h or as quickly as 10 min at 960 °C. The time needed to induce crystallization of the CMAS glass could be of the same order as infiltration time into the coating at sufficiently high temperatures. Further investigation of the temperature-dependent viscosity of this CMAS glass, its thermal properties and its thermochemical interactions with EBC materials is currently underway to determine if crystallization will indeed happen within the time frame needed for molten CMAS to infiltrate a coating.

3.4 Microstructural Evaluation of Heat Treated CMAS Glass

Figure 6 shows backscatter SEM micrographs of polished cross-sections of the heat treated bulk glass specimens exhibiting various extents of crystallization depending on the heat treatment. SEM backscatter micrographs revealed that crystallization initiated at the surface of CMAS bulk glass, regardless of whether in contact with platinum crucible or air, heat treated at 900 °C and above. No crystalline phases were observed in specimens heat treated ≤825 °C. These results supported the XRD observation described in Section 3.3 that the CMAS glass did not crystallize below 900 °C. Surface crystallization appeared to be the primary mechanism by which crystal growth occurred in heat treated CMAS specimens. This was consistent with DTA scans of glass powder and bulk specimens (shown in Fig. 2) discussed in Section 3.2 as well as with previous CMAS investigations of glasses with similar compositions (Refs. 15, 28, 31, and 32). The dendritic crystals appeared to develop at the surface and grow radially inward in the specimens examined.

As shown in Figure 6, the average thickness of the crystalline layer at the surface of heated CMAS glass bulk specimens increased with heat treatment temperature above 900 °C as well as with longer isothermal hold times at a given temperature. The average thicknesses of the crystalline layer are given in Table 4. The thicker surface layer of highly dendritic crystallites observed in specimens heated at 925 °C and above suggested that the rate of crystal growth increased with temperature. At heat treatments of 925 °C for 20 h and 960 °C for 5 h, crystallites fully spanned the thickness of the CMAS specimens, which indicated that these samples had the highest degree of crystallinity. The microstructures of CMAS glass specimens heat treated at 900 and 960 °C are shown in Figure 7. All specimens heated at and above 900 °C exhibited a similar microstructure near the sample surface. Well-formed crystal dendrites were readily observed in specimens with layers >30 μm in thickness heat treated above 900 °C, as shown in Figure 7. Darker regions that were observed near the surface in all specimens heat treated at 900 °C and above did not appear to develop further than ~30 μm into the sample from the surface.

Figures 8 and 9 show micrographs and EDS maps of polished cross-sections of specimens heated at 900 °C for 10 h and at 960 °C for 1 h, respectively, at the crystal growth front. EDS maps corresponding to silicon, aluminum and oxygen signals (not shown) exhibited uniform intensity throughout the crystalline and amorphous regions of the specimens, suggesting that these elements were present throughout the specimen. EDS analysis revealed that the darker areas of the crystal layer near the surface of the samples, clearly visible in Figures 7 and 8, contained magnesium, while the lighter areas of the crystal layer, seen in Figures 7 to 9, were calcium rich. This suggested that the lighter crystals corresponded to a calcium silicate ($CaSiO_3$) phase, since higher calcium signals were observed in comparison with the other elements detected. The darker crystalline regions near the surface observed in all specimens heat treated at and above 900 °C (shown in backscatter SEM micrographs in Fig. 7) likely corresponded to a calcium-magnesium aluminosilicate phase, as EDS maps reflected a higher magnesium signal from those areas.

SEM and EDS analysis suggested that the darker crystalline regions observed in the partially crystalline specimens contained magnesium (refer to backscatter SEM micrograph and EDS maps in Fig. 8). Although sodium-containing phases were not detected by XRD, EDS mapping of the uncrystallized bulk and grain boundaries indicated a higher sodium content than in the crystallized surface region, as shown in Figures 8 and 9. If sodium remained within the amorphous regions and along the grain boundaries, it likely would not be detected by XRD.

4.0 Summary and Conclusions

The crystallization kinetics of CMAS glass powder and bulk specimens was evaluated using DTA. Two distinct exothermic peaks, which suggested the likely precipitation of two crystalline phases, were observed at ~840 to 930 °C and 901 to 1024 °C in DTA thermograms of the glass powder. Activation energies for the first and second peaks were 263 and 294 kJ/mol, and frequency factors were 4.87×10^{8} s^{-1} and 1.29×10^{10} s^{-1}. Only one exothermic peak at ~1054 to 1167 °C was clearly observed in all DTA scans of bulk glass specimens. An activation energy value of 286 kJ/mol and a frequency factor of 3.70×10^{8} s^{-1}

were determined for this peak, which corresponded to the second exothermic peak in DTA of glass powder. The significant shift in the second exothermic peak in DTA scans from ~901 to 1024 °C in glass powder to ~1054 to 1167 °C in bulk glass likely suggested a surface-nucleated mechanism for crystallization in CMAS glass.

XRD spectra of glass bulk specimens heat treated at ≥900 °C showed the development of wollastonite ($CaSiO_3$) as a primary crystalline phase. Aluminum diopside ($Ca(Mg,Al)(Si,Al)_2O_6$) was also detected as a minor phase in specimens heated at >900 °C. Microstructural evaluation by SEM/EDS confirmed the presence of compositions corresponding to wollastonite and aluminum diopside crystals that initiated from the surface and grew radially inward in glass specimens heated at and above 900 °C. The thickness of the crystalline layer increased with temperature as well as hold time. Sodium content was restricted to the amorphous region and in between crystallites. Understanding of the crystallization behavior of CMAS compositions may help to mitigate damage to protective T/EBC coatings through initiation of CMAS crystallization.

References

1. De Wet D., Taylor R., Stott F. Corrosion mechanisms of ZrO2-Y2O3 thermal barrier coatings in the presence of molten middle-east sand. *Le Journal de Physique IV* 1993;3(C9):C9-655-C9-63.
2. Stott FH., de Wet DJ., Taylor R. Degradation of Thermal-Barrier Coatings at Very High Temperatures. *MRS Bulletin* 1994;19(10):46-49.
3. Spitsberg I., Steibel J., Thermal and Environmental Barrier Coatings for SiC/SiC CMCs in Aircraft Engine Applications*. *International Journal of Applied Ceramic Technology* 2004;1(4):291-301.
4. Levi CG, Hutchinson JW, Vidal-Sétif M-H, Johnson CA. Environmental degradation of thermal-barrier coatings by molten deposits. *MRS bulletin* 2012;37(10):932-41.
5. Grant KM, Krämer S, Löfvander JPA, Levi CG. CMAS degradation of environmental barrier coatings. *Surface and Coatings Technology* 2007;202(4–7):653-57.
6. Ahlborg NL, Zhu D. Calcium–magnesium aluminosilicate (CMAS) reactions and degradation mechanisms of advanced environmental barrier coatings. *Surface and Coatings Technology* 2013;237(0):79-87.
7. Harder BJ, Ramìrez-Rico J, Almer JD, Lee KN, Faber KT. Chemical and Mechanical Consequences of Environmental Barrier Coating Exposure to Calcium–Magnesium–Aluminosilicate. *Journal of the American Ceramic Society* 2011;94s178-s85.
8. Krämer S, Faulhaber S, Chambers M, Clarke DR, Levi CG, Hutchinson JW, Evans AG. Mechanisms of cracking and delamination within thick thermal barrier systems in aero-engines subject to calcium-magnesium-alumino-silicate (CMAS) penetration. *Materials Science and Engineering: A* 2008;490(1–2):26-35.
9. Borom MP, Johnson CA, Peluso LA. Role of environment deposits and operating surface temperature in spallation of air plasma sprayed thermal barrier coatings. *Surface and Coatings Technology* 1996;86–87, Part 1(0):116-26.
10. Evans AG, Hutchinson JW. The mechanics of coating delamination in thermal gradients. *Surface and Coatings Technology* 2007;201(18):7905-16.
11. Mercer C, Faulhaber S, Evans AG, Darolia R. A delamination mechanism for thermal barrier coatings subject to calcium–magnesium–alumino-silicate (CMAS) infiltration. *Acta Materialia* 2005;53(4):1029-39.
12. Aygun A, Vasiliev AL, Padture NP, Ma X. Novel thermal barrier coatings that are resistant to high-temperature attack by glassy deposits. *Acta Materialia* 2007;55(20):6734-45.
13. Drexler JM, Shinoda K, Ortiz AL, Li D, Vasiliev AL, Gledhill AD, Sampath S, Padture NP. Air-plasma-sprayed thermal barrier coatings that are resistant to high-temperature attack by glassy deposits. *Acta Materialia* 2010;58(20):6835-44.

14. Gledhill AD, Reddy KM, Drexler JM, Shinoda K, Sampath S, Padture NP. Mitigation of damage from molten fly ash to air-plasma-sprayed thermal barrier coatings. *Materials Science and Engineering: A* 2011;528(24):7214-21.
15. Keyvani N, Marghussian VK, Rezaie HR, Kord M. Effect of Al2O3 Content on Crystallization Behavior, Microstructure, and Mechanical Properties of SiO2–Al2O3–CaO–MgO Glass–Ceramics. *International Journal of Applied Ceramic Technology* 2011;8(1):203-13.
16. Reddy AA, Goel A, Tulyaganov DU, Kapoor S, Pradeesh K, Pascual MJ, Ferreira JMF. Study of calcium–magnesium–aluminum–silicate (CMAS) glass and glass-ceramic sealant for solid oxide fuel cells. *Journal of Power Sources* 2013;231(0):203-12.
17. Barbieri L, Corradi A, Lancellotti I. Thermal and chemical behaviour of different glasses containing steel fly ash and their transformation into glass-ceramics. *Journal of the European Ceramic Society* 2002;22(11):1759-65.
18. Torres FJ, Alarcón J. Pyroxene-based glass-ceramics as glazes for floor tiles. *Journal of the European Ceramic Society* 2005;25(4):349-55.
19. McMillan PW. The crystallisation of glasses. *Journal of Non-Crystalline Solids* 1982;52(1–3):67-76.
20. Bansal NP, Doremus RH. Determination of reaction kinetic parameters from variable temperature DSC or DTA. *Journal of thermal analysis* 1984;29(1):115-19.
21. Bansal NP, Doremus RH, Bruce AJ, Moynihan CT. Kinetics of Crystallization of ZrF4-Ba2-LaF3 Glass by Differential Scanning Calorimetry. *Journal of the American Ceramic Society* 1983;66(4):233-38.
22. Bansal NP, Bruce AJ, Doremus RH, Moynihan CT. The influence of glass composition on the crystal growth kinetics of heavy metal fluoride glasses. *Journal of non-crystalline solids* 1985;70(3):379-96.
23. Avrami M. Kinetics of phase change. I General theory. *The Journal of Chemical Physics* 1939;7(12):1103-12.
24. Avrami M. Granulation, phase change, and microstructure kinetics of phase change. III. *The Journal of Chemical Physics* 1941;9(2):177-84.
25. Avrami M. Kinetics of Phase Change. II. Transformation-time relations for random distribution of nuclei. *Journal of Chemical Physics* 1940;8212-24.
26. Johnson WA, Mehl RF. Reaction kinetics in processes of nucleation and growth. *Trans. Aime* 1939;135(8):396-415.
27. Borchardt HJ. Initial reaction rates from DTA. *Journal of Inorganic and Nuclear Chemistry* 1960;12(3–4):252-54.
28. Barbieri L, Bondioli F, Lancellotti I, Leonelli C, Montorsi M, Ferrari AM, Miselli P. The Anorthite–Diopside System: Structural and Devitrification Study. Part II: Crystallinity Analysis by the Rietveld–RIR Method. *Journal of the American Ceramic Society* 2005;88(11):3131-36.
29. Bansal NP, Choi SR. Properties of Desert Sand and CMAS Glass. Article in review.
30. Piloyan G, Ryabchikov I, Novikova O. Determination of activation energies of chemical reactions by differential thermal analysis. 1966.
31. Barbieri L, Corradi A, Lancellotti I, De Oliveira APN, Alarcon OE. Nucleation and Crystal Growth of a MgO–CaO–Al2O3–SiO2Glass with Added Steel Fly Ash. *Journal of the American Ceramic Society* 2002;85(3):670-74.
32. Leonelli C, Manfredini T, Paganelli M, Pozzi P, Pellacani GC. Crystallization of some anorthite-diopside glass precursors. *J Mater Sci* 1991;26(18):5041-46.

TABLE 1.—PEAK MAXIMUM TEMPERATURES FOR THE FIRST AND/OR SECOND EXOTHERMIC PEAKS OBTAINED BY DTA OF CMAS GLASS POWDER (T_{P1} AND T_{P2}, RESPECTIVELY) AND BULK SPECIMENS (T_{B2}) AT VARYING SCAN RATES (θ)

	Powder		Bulk
Scan rate, θ [°C/min]	T_{P1} [°C]	T_{P2} [°C]	T_{B2} [°C]
5	842.1	929.5	1054.2
10	861.1	954.4	1069.8
20	893.5	980.5	1108.4
30	910.7	999.7	1137.4
40	920	1012.4	1146.5
50	930	1024.4	1166.9

TABLE 2.—ACTIVATION ENERGY AND FREQUENCY FACTOR VALUES FOR CRYSTALLIZATION OF CMAS GLASS POWDER AND BULK SPECIMENS DETERMINED BY DTA

Parameter	Powder	Bulk
Activation Energy for Peak 1, E_1 [kJ/mol]	263	----------
Activation Energy for Peak 2, E_2 [kJ/mol]	294	286
Frequency Factor for Peak 1, ν_1 [s^{-1}]	4.87×10^{9}	----------
Frequency Factor for Peak 2, ν_2 [s^{-1}]	1.29×10^{10}	3.70×10^{8}

TABLE 3.—DEVELOPMENT OF CRYSTALLINE PHASES IN CMAS GLASS BULK SPECIMENS AFTER DIFFERENT HEAT TREATMENTS

Heat treatment		Crystalline phases detected from XRD		
Temperature, °C	Time	Amorphous	Wollastonite[a] ($CaSiO_3$)	Aluminum diopside[b] ($Ca(Mg,Al)(Si,Al)_2O_6$)
800	10 h	X	--	--
825	10 h	X	--	--
900	10 h	X	X	?
925	10 h	X	X	X
925	20 h	X	X	X
960	10 min	X	X	X
960	1 h	X	X	X
960	5 h	--	X	X

[a]PDF 04-010-0710 wollastonite
[b]PDF 01-076-2502 aluminum diopside

TABLE 4.—THICKNESS OF CRYSTALLINE LAYER THAT DEVELOPED IN CMAS GLASS BULK SPECIMENS HEAT TREATED AT VARIOUS TEMPERATURES FOR VARYING DURATIONS

Temperature, °C	Time	Crystal layer thickness, μm
900	10 h	25.6±10.3
925	10 h	97.5±8.3
925	20 h	Through specimen thickness of ~4 mm
960	10 min	47.9±6.4
960	1 h	367.2±13.9
960	5 h	Through specimen thickness of ~4 mm

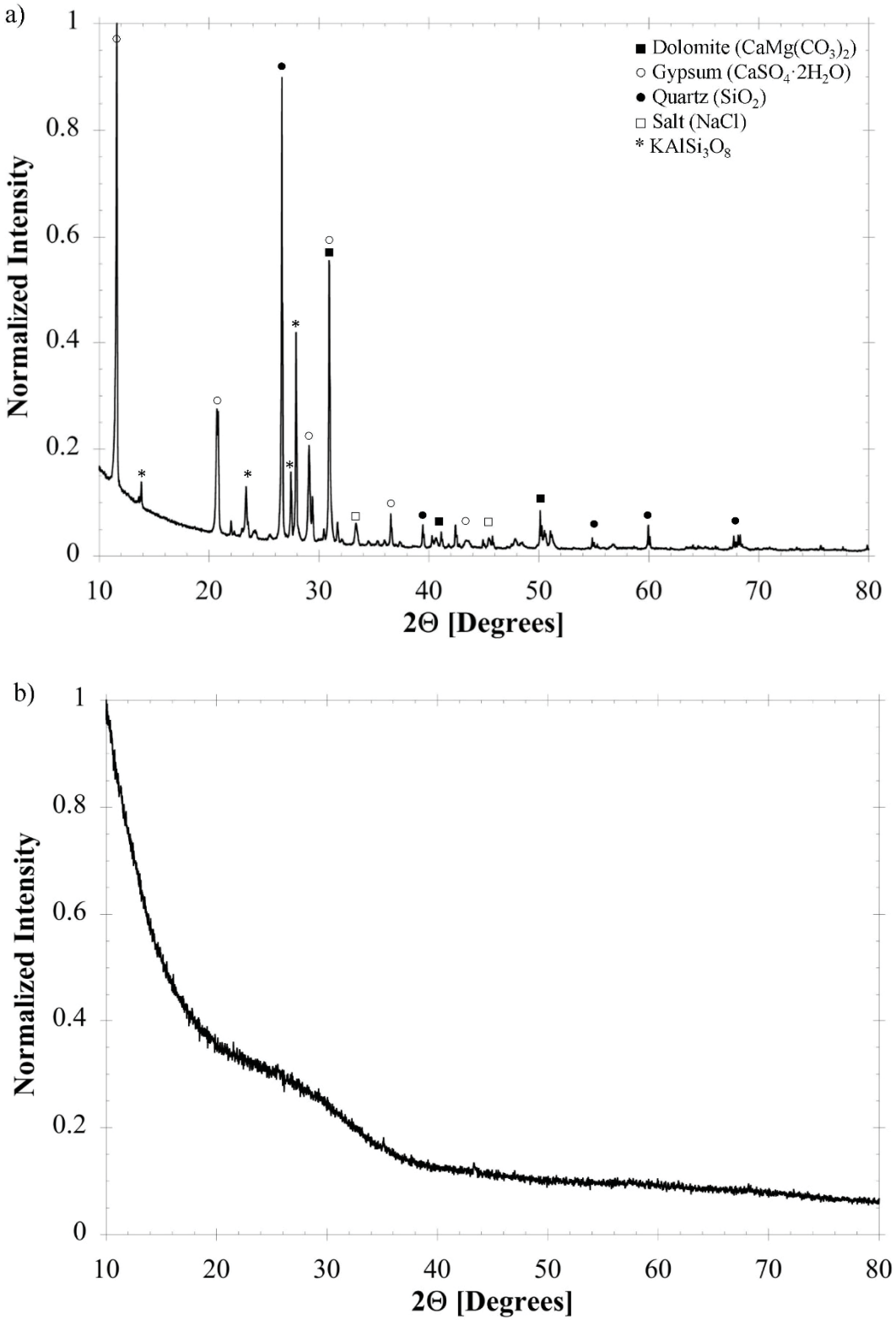

Figure 1.—XRD spectra of (a) synthetic sand and (b) the CMAS glass powder.

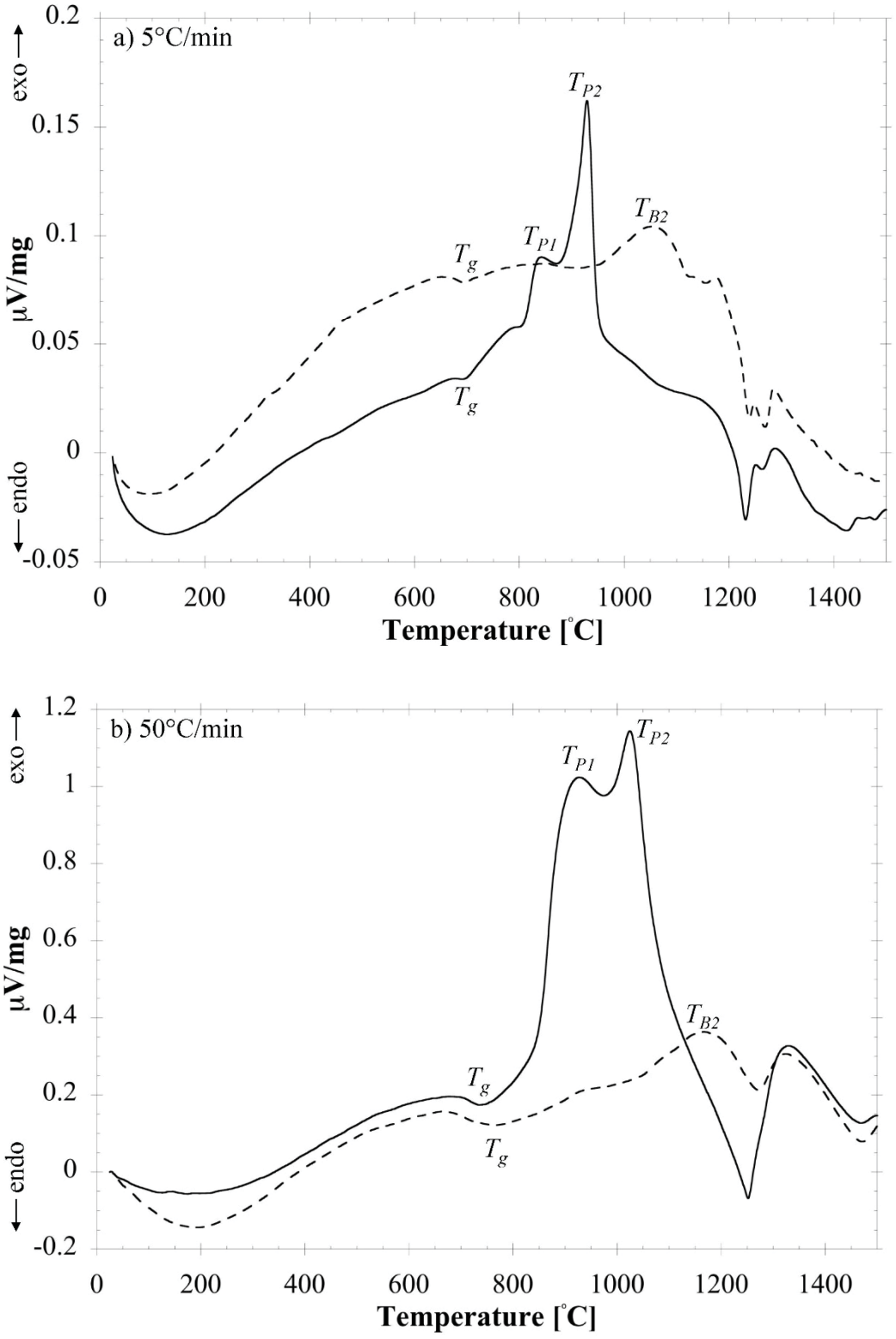

Figure 2.—Differential thermal analysis scans of CMAS glass powder (solid line) and bulk specimens (dashed line) obtained at heating rates of (a) 5 °C/min and (b) 50 °C/min.

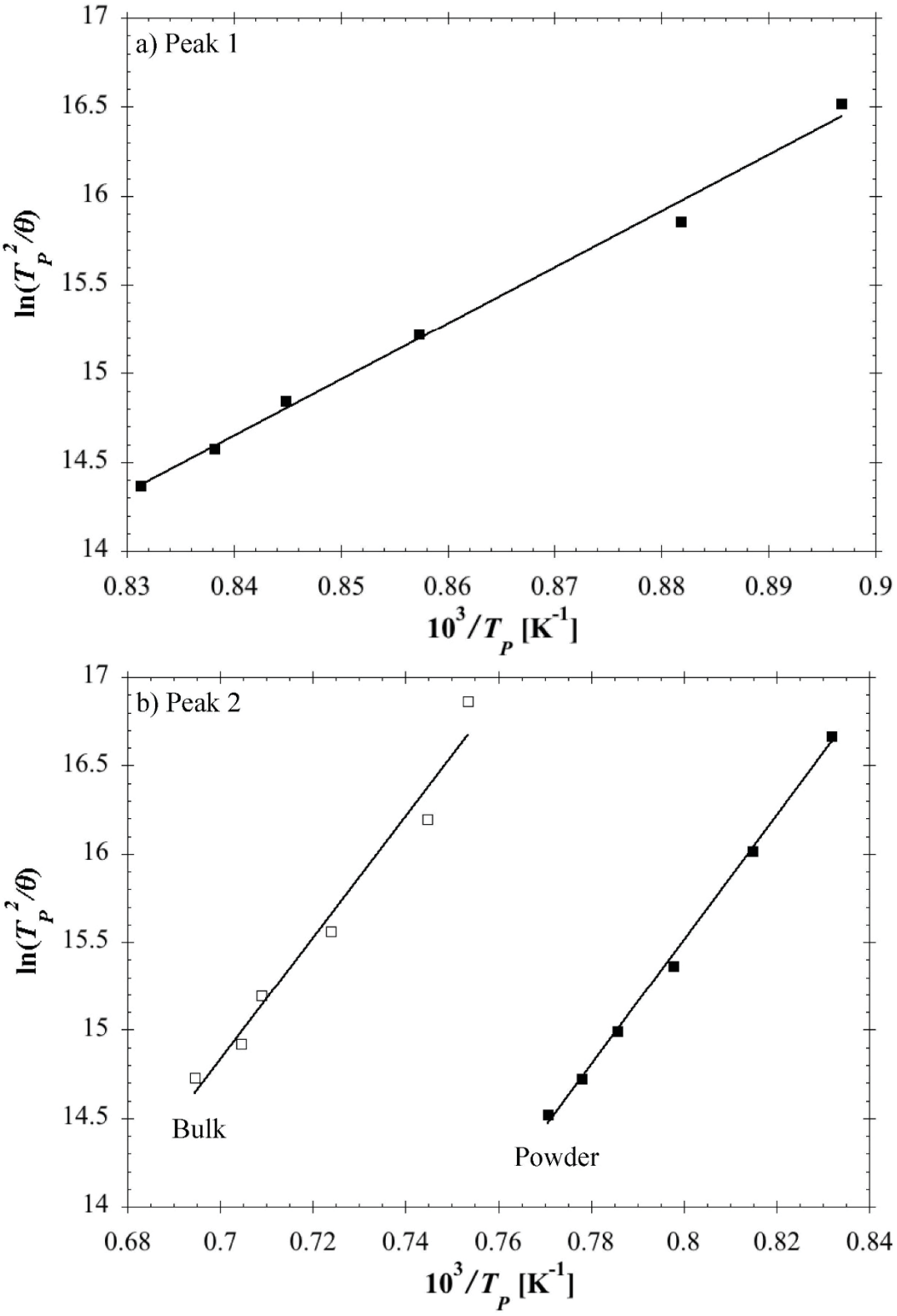

Figure 3.—Plots of $\ln(T_P^2/\theta)$ versus reciprocal crystallization peak maximum temperature for the (a) first and (b) second crystallization peaks for CMAS glass powder (■) and bulk (□).

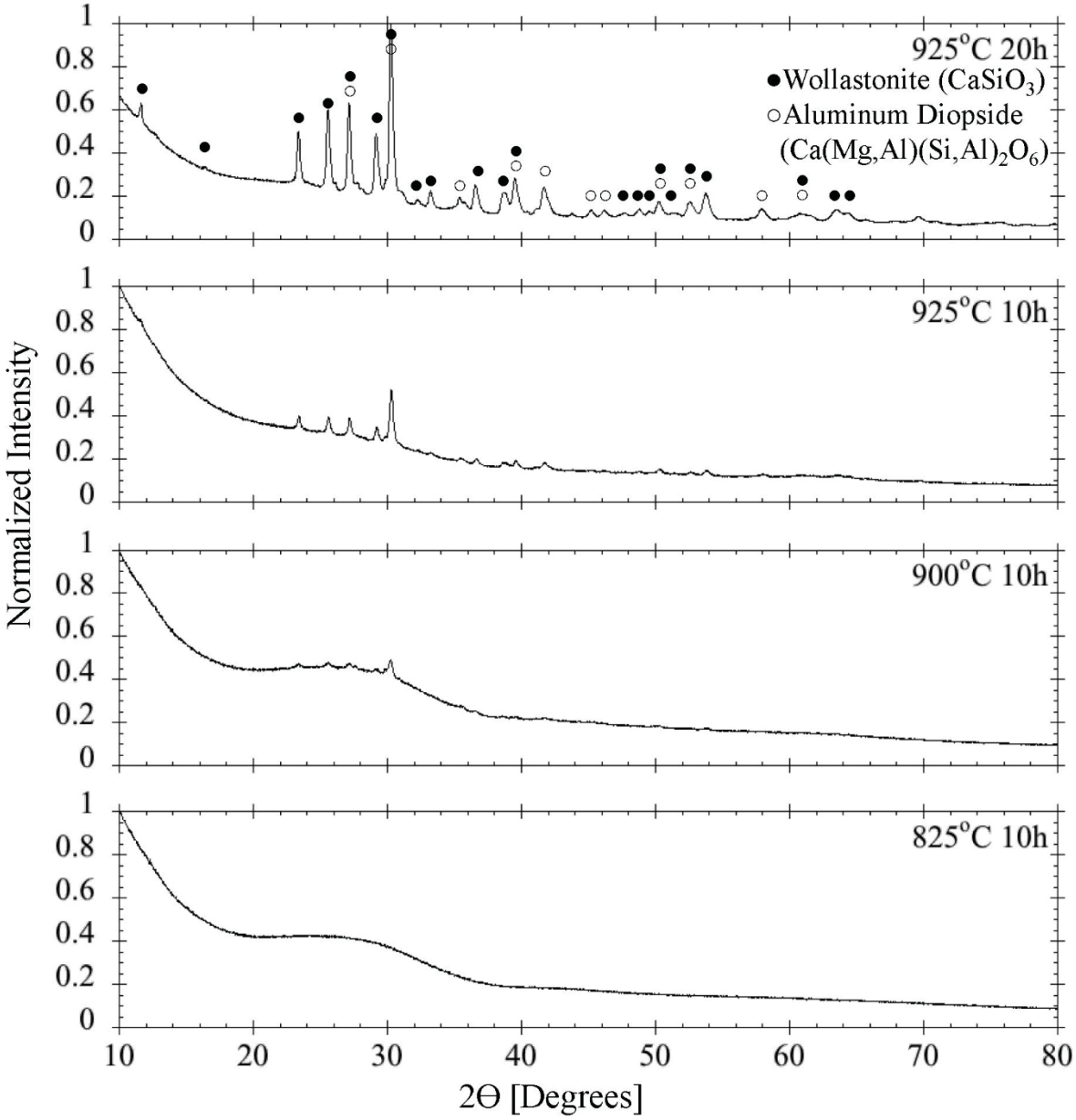

Figure 4.—Powder XRD spectra of CMAS bulk glass heat treated at temperatures ranging from 825 to 925 °C for various hold times.

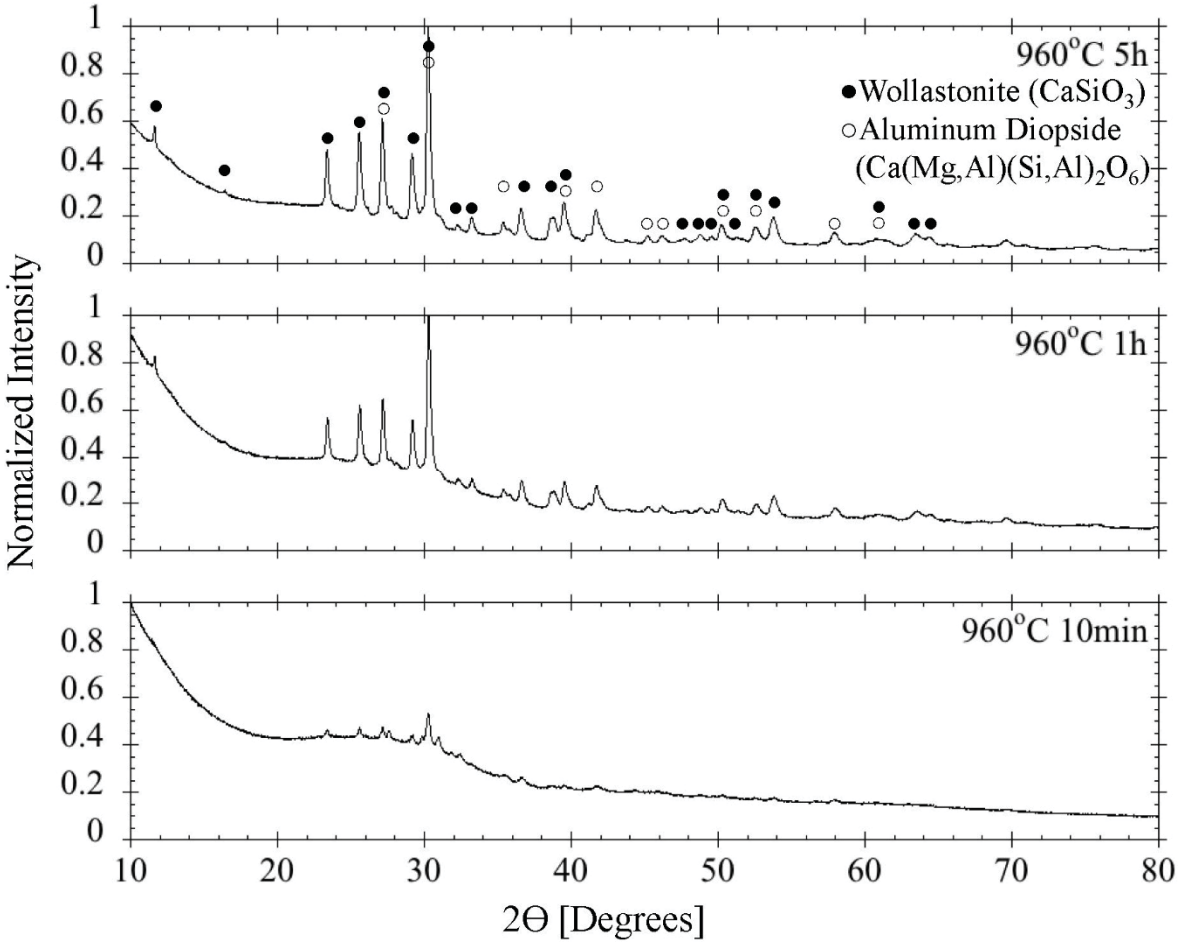

Figure 5.—Powder XRD spectra of CMAS bulk glass heat treated at 960 °C for various hold times.

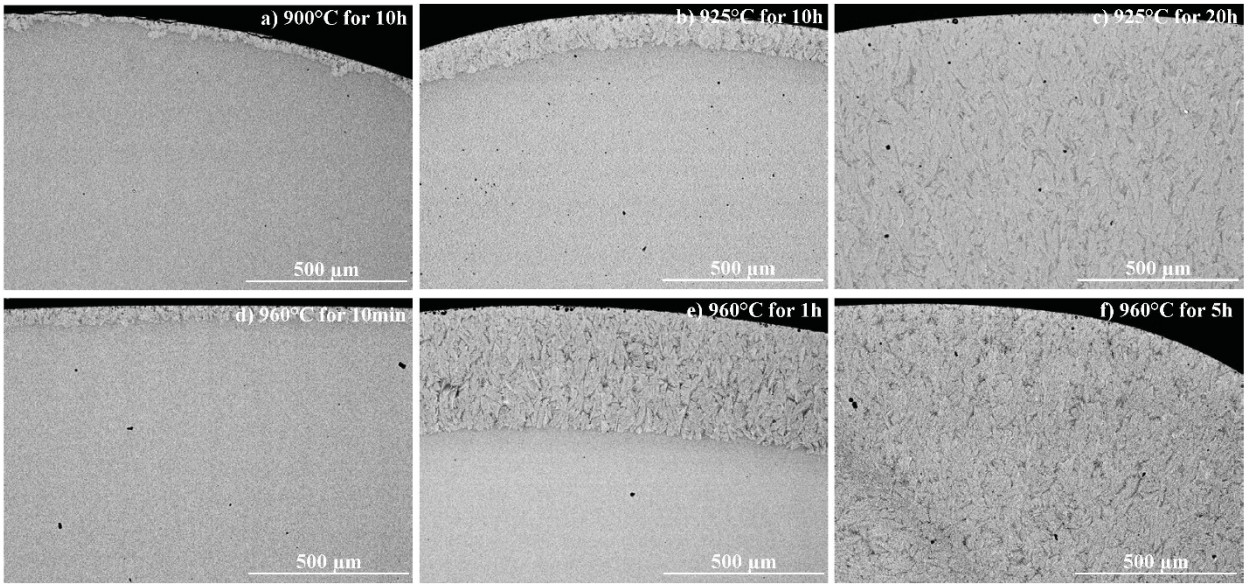

Figure 6.—Backscatter SEM micrographs showing polished cross-sections of CMAS glass bulk specimens heat treated at (a) 900 °C for 10 h, (b) 925 °C for 10 h, (c) 925 °C for 20 h, (d) 960 °C for 10 min, (e) 960 °C for 1 h and (f) 960 °C for 5 h.

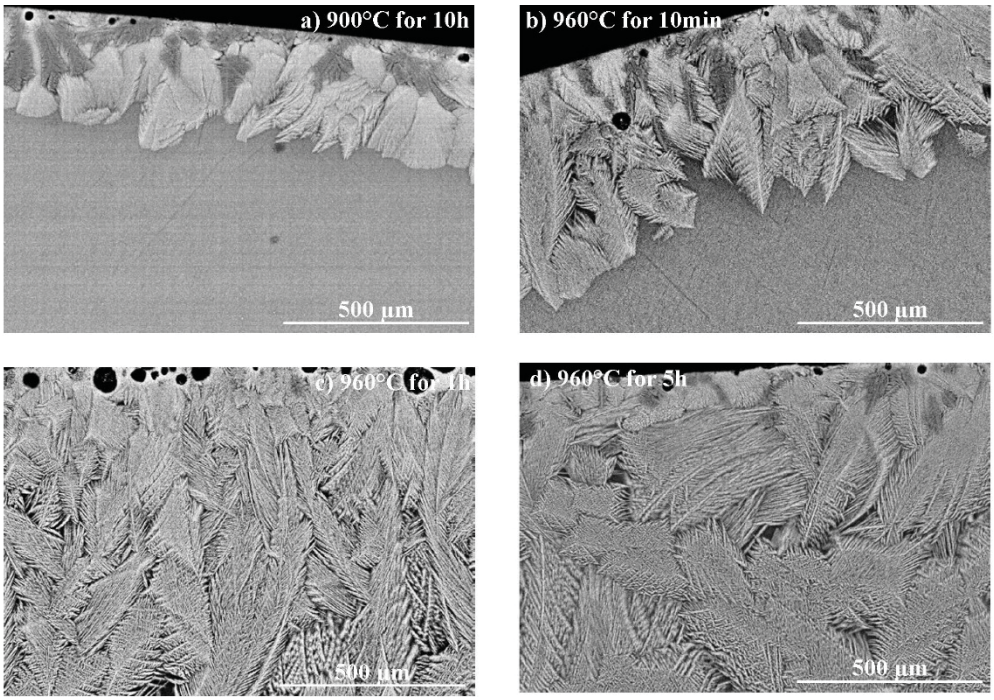

Figure 7.—Backscatter SEM micrographs showing polished cross-sections of CMAS glass bulk specimens heat treated at (a) 900 °C for 10 h, (b) 960 °C for 10 min, (c) 960 °C for 1 h and (d) 960 °C for 5 h.

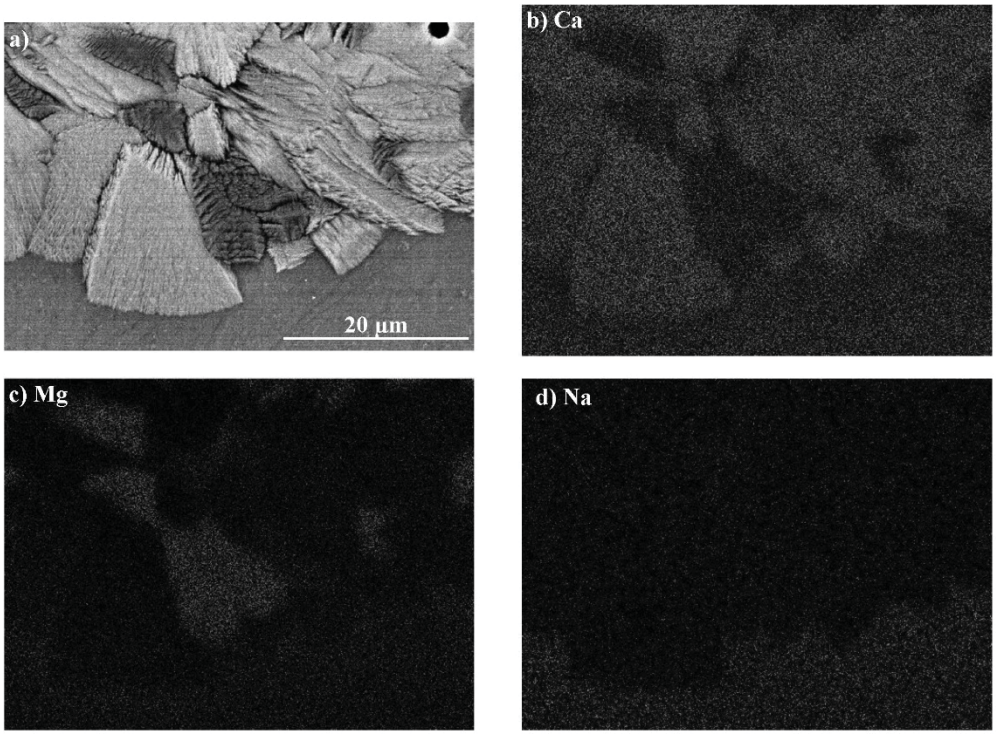

Figure 8.—EDS maps for a polished cross-section of CMAS glass bulk specimen heat treated at 900 °C for 10 h. (a) Backscatter SEM micrograph and corresponding elemental maps of (b) calcium, (c) magnesium and (d) sodium.

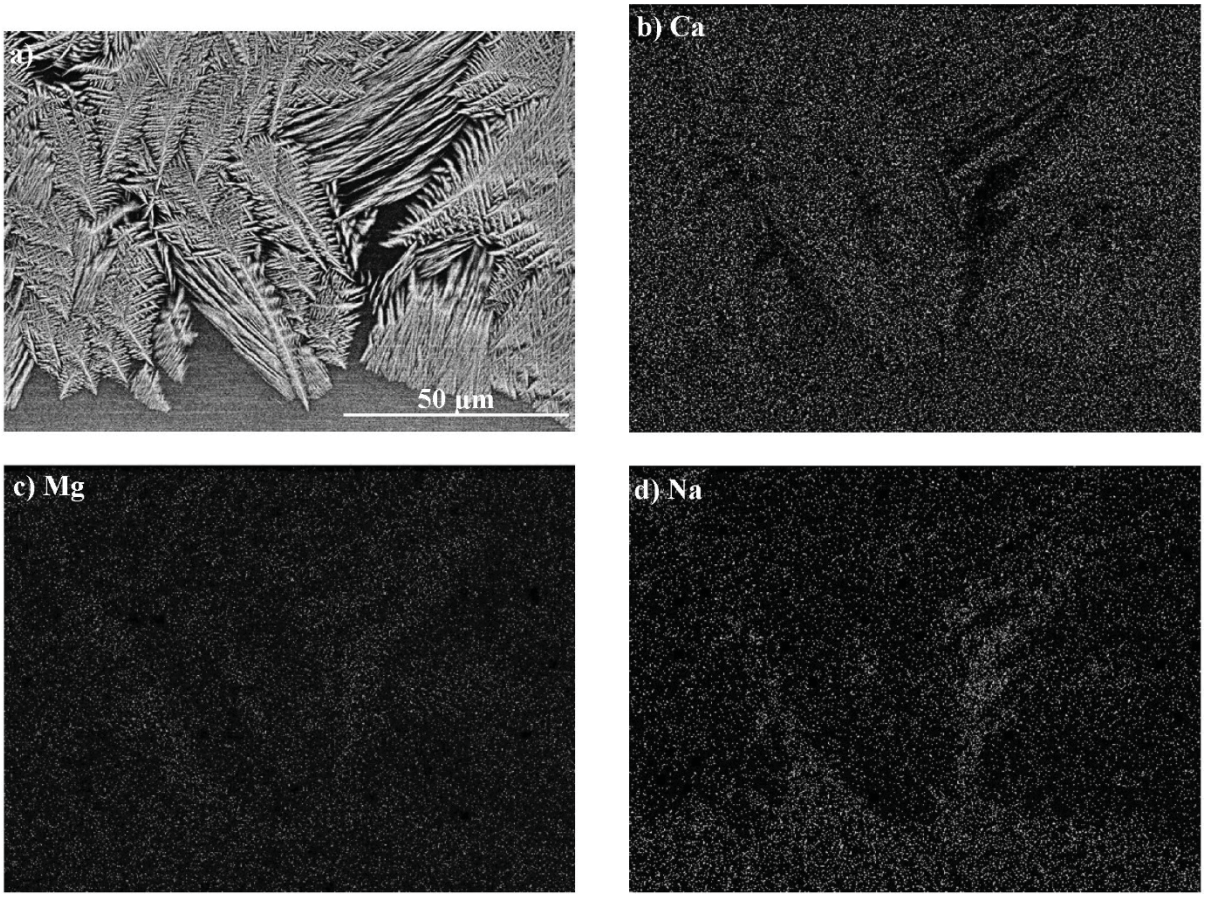

Figure 9.—EDS maps for a polished cross-section of CMAS glass bulk specimen heat treated at 960 °C for 1 h. (a) Backscatter SEM micrograph and corresponding elemental maps of (b) calcium, (c) magnesium and (d) sodium.